Contribution from the Institut für Anorganische Chemie,
Universität Bern, Freiestrasse 3, 3000 Bern 9, Switzerland

Synthesis and Spectroscopic Properties of Praseodymium(III) Acetate Hydrate

Markus P. Hehlen, Hans Riesen,† and Hans U. Güdel*

Received November 9, 1990

A new synthesis for the quasi-one-dimensional compound $Pr(CH_3COO)_3 \cdot H_2O$ and its deuterated analogue $Pr(CD_3COO)_3 \cdot D_2O$ is reported. Well-resolved absorption, luminescence, and Raman measurements on single crystals of these compounds as well as the diluted system $Ce(CH_3COO)_3 \cdot H_2O$:1% Pr^{3+} down to 5 K are reported and analyzed. Due to high-energy O–H stretching vibrations of the directly coordinated water molecule, excited states are efficiently depopulated by nonradiative multiphonon relaxation. In the concentrated crystal, the relaxation rate of the $^3P_0$ excited state at 5 K is $\sim 2 \times 10^8$ s^{-1} and $>10^9$ s^{-1} for the deuterated and nondeuterated compound, respectively. In addition, cross relaxation contributes to the nonradiative depopulation of the $^1D_2$ excited state. It is thus likely that energy migration along the chain is not important. The $^3H_4 \rightarrow {}^3P_0$ absorption has a relatively intense sideband, 65% and 20% of the total intensity for $Pr(CH_3COO)_3 \cdot H_2O$ and $Ce(CH_3COO)_3 \cdot H_2O$:1% Pr^{3+}, respectively. Double excitations involving nearest neighbors in the chain contribute two-thirds of the sideband intensity of the undiluted compound, one-third being vibronic.

1. Introduction

An important parameter for the relaxation dynamics of metal ions in solids is the dimensionality of the system. A one-dimensional system imposes the highest restriction on ion–ion interactions, and energy migration that depends on such interactions between nearest neighbors in the lattice will thus be dominant in the chain direction. Such systems may show typical nonexponential decay characteristics of excited electronic states due to excitation energy migration along the chains to built-in acceptors.[1,2] To date, these effects have been experimentally investigated for trivalent lanthanide ions mainly on ionic compounds.[3-9]

In this paper, we present an investigation of the quasi-one-dimensional molecular compound $Pr(CH_3COO)_3 \cdot H_2O$. Acetates of trivalent lanthanides are known as acetate hydrates $Ln(CH_3COO)_3 \cdot zH_2O$ or as acetate hydrate chlorides $[Ln(CH_3COO)_x(H_2O)_y]Cl_{3-x} \cdot zH_2O$ (Ln = Ce^{3+}–Lu^{3+}). In all these compounds, the acetate ligand can act as a bridge between two Ln^{3+} ions, resulting in dimer or chain structures according to the following scheme:[10-15]

	$Ln(CH_3COO)_3 \cdot zH_2O$	$[Ln(CH_3COO)_x(H_2O)_y]Cl_{3-x} \cdot zH_2O$
dimer	Ln = Eu^{3+},[10,11] Gd^{3+},[12] Ho^{3+},[13] Tm^{3+}[11]	Ln = Pr^{3+}[14]
chain	Ln = Ce^{3+},[11] Pr^{3+},[10] Nd^{3+}[11]	Ln = Eu^{3+}[15]

In all these compounds, Ln^{3+} is 9-fold oxygen-coordinated and water is found as a first-sphere ligand. The structure of $Pr(CH_3COO)_3 \cdot H_2O$ has been determined and shows a pronounced one-dimensionality with an interchain distance of 7.8 Å and a nearest intrachain Pr^{3+}–Pr^{3+} distance of 4.4 Å.[10] Neighboring Pr^{3+} ions within the chains are bridged by acetate ligands. A water molecule completes the coordination, leading to a coordination number of 9. The point symmetry of Pr^{3+} is C_1.

Energy migration along the chain will be in competition with radiative and nonradiative single-ion relaxation processes. For $Pr(CH_3COO)_3 \cdot H_2O$, the nonradiative competing processes are expected to be very efficient for two reasons:

The relatively small energy gaps between excited 4f states and the presence of high-energy O–H stretching vibrations of the directly coordinated water molecule may cause a very high multiphonon relaxation rate.

Interactions with neighboring Pr^{3+} ions may lead to efficient nonradiative processes such as cross relaxation.[16]

Whether effects of long-range energy migration to acceptors can be observed or not will depend on the relative magnitude of these competing rates and the energy-transfer rate.

2. Experimental Section

Synthesis and Crystal Growth. A 2.5-g sample of $PrCl_3 \cdot 7H_2O$ (Janssen, 99.9%) was dissolved in water. Praseodymium hydroxide was precipitated by adding a 25% NH_3 solution (Merck p.a.) dropwise, filtered off through a 10 μm glass filter and redissolved by adding 4 mL of glacial acetic acid (Merck p.a.). After this procedure was repeated three times, light green single crystals of $Pr(CH_3COO)_3 \cdot H_2O$ were obtained by isothermal evaporation of the solution at room temperature. The crystals were checked by X-ray powder diffraction.

For the deuterated compound, the following new synthesis was developed. Needles of $Pr(CD_3COO)_3 \cdot D_2O$ were grown by refluxing 1.5 g of anhydrous Pr_6O_{11} (Fluka puriss), 20 mL of glacial acetic acid-d_4 (Merck, 99%), and 1 mL of D_2O (Merck, 99.75%) for 36 h. Single-crystal growth was observed at the surface of undissolved Pr_6O_{11} particles. The X-ray powder pattern corresponds to the pattern of the undeuterated compound.

Single crystals of $Ce(CH_3COO)_3 \cdot H_2O$:1% Pr^{3+} were obtained from a saturated solution of $Ce(CH_3COO)_3 \cdot zH_2O$ (Johnson Matthey, 99.99%) and 1% praseodymium hydroxide in 96% acetic acid (Merck p.a.) over KOH in an desiccator at room temperature.

Spectroscopic Measurements. Polarized single-crystal absorption measurements were done on a modified Cary 17 spectrophotometer. The polarization was defined by using the crystal's *b* axis, with the electric vector *E* parallel to *b* as π polarization and *E* perpendicular to *b* as σ polarization. Luminescence and Raman spectra were measured by using an Ar^+ laser (Spectra Physics 2040). The luminescence was dispersed by a 0.85-m double monochromator Spex 1402 with 500-nm blazed 1200 grooves/mm gratings and detected by a photomultiplier (RCA 31034) using a photon counting system (Spex DPC-2). Nanosecond lifetime measurements were performed by using a dye laser (Lambda Physics FL3002, Coumarin 47 (Radiant Dyes Chemie) in methanol; oscillator 1.3×10^{-3}M; amplifier 2.6×10^{-3}M) pumped by a Nd:YAG laser (Quanta Ray DCR-3) giving 10-ns pulses at 20 Hz. The luminescence was analyzed by using a fast preamplifier (Stanford Research SR440) and a photodiode triggered oscilloscope (Tektronix 2430A). The lifetime was estimated by a numerical deconvolution of the signal, assuming a single exponential decay. Sample cooling was achieved with a helium gas flow-tube. For data acquisition and monochromator control, a microcomputer system (Tektronix 4052A) was used. The reported spectra

† Present address: Research School of Chemistry, Australian National University, G.P.O. Box 4, Canberra, ACT 2601, Australia.

(1) Movaghar, B.; Sauer, G. W.; Würtz, D. *J. Stat. Phys.* **1982**, *27*, 473.
(2) Agmon, N. *J. Stat. Phys.* **1986**, *43*, 537.
(3) Garapon, C. T.; Jacquier, B.; Chaminade, J. P.; Fouassier, C. *J. Lumin.* **1985**, *34*, 211.
(4) Buijs, M.; Blasse, G. *J. Lumin.* **1986**, *34*, 263.
(5) Buijs, M.; Blasse, G. *J. Lumin.* **1986**, *35*, 213.
(6) Buijs, M.; Blasse, G. *Chem. Phys. Lett.* **1987**, *137*, 381.
(7) Buijs, M.; Blasse, G. *J. Lumin.* **1988**, *39*, 323.
(8) Mahiou, R.; Metin, J.; Fournier, M. T.; Cousseins, J. C. *J. Lumin.* **1989**, *43*, 51.
(9) Tian, F. W.; Fouassier, C.; Hagenmüller, P. *J. Phys. Chem. Solids* **1987**, *48*, 245.
(10) Ganapathy, S.; Chacko, V. P.; Bryant, R. G.; Etter, M. C. *J. Am. Chem. Soc.* **1990**, *108*, 12.
(11) Fuchs, F. R. Thesis, University of Tübingen, Tübingen, FRG, 1983.
(12) Favas, M. C.; Kepert, D. L.; Skelton, B. W.; White, A. H. *J. Chem. Soc., Dalton Trans.* **1980**, *1*, 454.
(13) Bats, J. W.; Kalus, R.; Fuess, H. *Acta Crystallogr.* **1979**, *B35*, 1225.
(14) Schleid, T.; Meyer, G. *Z. Anorg. Allg. Chem.* **1990**, *583*, 46.
(15) Schleid, T.; Meyer, G. *Z. Naturforsch.* **1989**, *44B*, 1007.
(16) Dornauf, H.; Heber, J. *J. Lumin.* **1980**, *22*, 1.

0020-1669/91/1330-2273$02.50/0

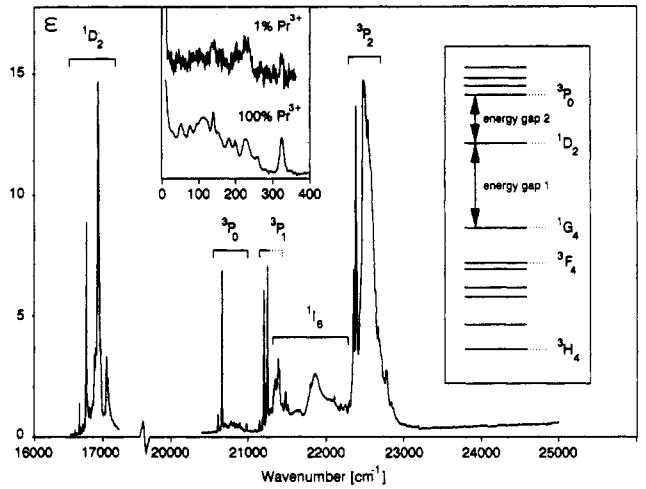

Figure 1. Unpolarized absorption of $Pr(CD_3COO)_3 \cdot D_2O$ at 40 K. The notation is given in Russel–Saunders terms of the free Pr^{3+} ion, the electronic states of which are schematically shown on the right-hand side. The insert on top compares the $^3H_4 \rightarrow {}^3P_0$ sideband structure of $Pr(CH_3COO)_3 \cdot H_2O$ and $Ce(CH_3COO)_3 \cdot H_2O$:1% Pr^{3+}; the two spectra are scaled.

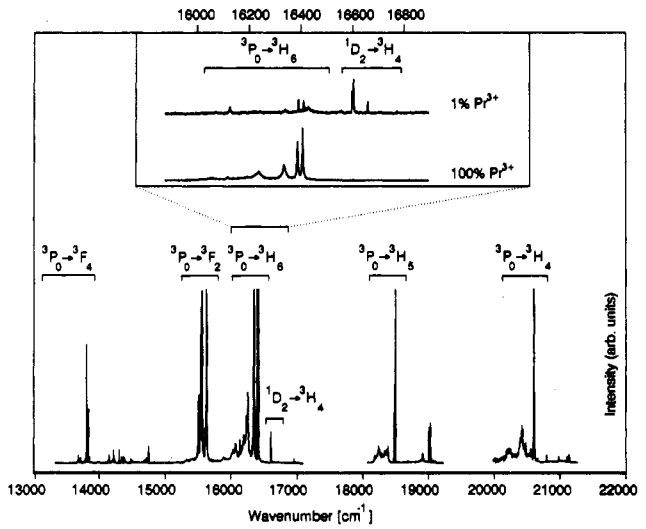

Figure 2. Unpolarized luminescence of $Pr(CD_3COO)_3 \cdot D_2O$ at 7 K. The insert shows the strong concentration dependence of the relative intensities of $^3P_0$ and $^1D_2$ in $Pr(CH_3COO)_3 \cdot H_2O$ and $Ce(CH_3COO)_3 \cdot H_2O$:1% Pr^{3+}. The intensity scales of the three spectra are different.

are not corrected for the wavelength dependence of the instrumental response.

3. Results

Figure 1 shows the unpolarized visible absorption spectrum of $Pr(CD_3COO)_3 \cdot D_2O$ at 40 K. With its richly structured weak transitions having line widths of a few wavenumbers, it has the typical appearance of a Ln^{3+} spectrum. But the spectrum also shows broad bands with much more intensity, which are less typical of f–f transitions in trivalent lanthanides.[17,18] The identification of the observed groups of lines in $Pr(CD_3COO)_3 \cdot D_2O$ can be clearly made by a comparison with the calculated energies of the free Pr^{3+} ion[19] and with the spectra of Pr^{3+} in other compounds. The insert on top of Figure 1 shows a comparison of the $^3H_4 \rightarrow {}^3P_0$ low-energy sideband structure for $Pr(CH_3COO)_3 \cdot H_2O$ and the diluted crystal $Ce(CH_3COO)_3 \cdot H_2O$:1% Pr^{3+}. The undiluted compound has 65% of its total $^3H_4 \rightarrow {}^3P_0$ intensity in the sideband,

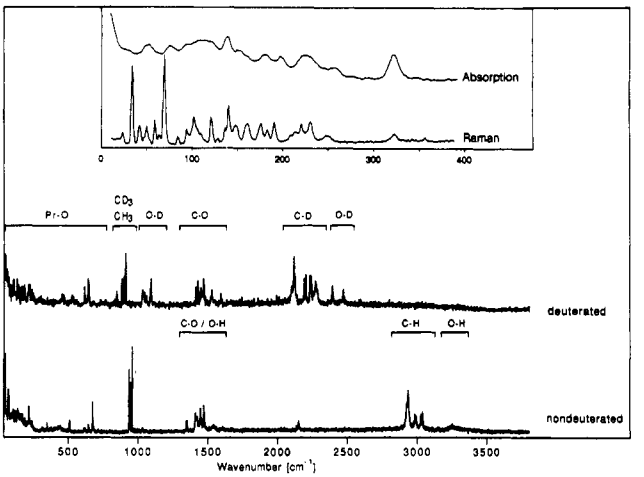

Figure 3. Raman spectra of $Pr(CH_3COO)_3 \cdot H_2O$ and $Pr(CD_3COO)_3 \cdot D_2O$ at 7 K with 488-nm excitation. The insert compares the low-energy region of the Raman spectrum with the sideband of the $^3H_4 \rightarrow {}^3P_0$ absorption relative to $^3H_4(0) \rightarrow {}^3P_0$.

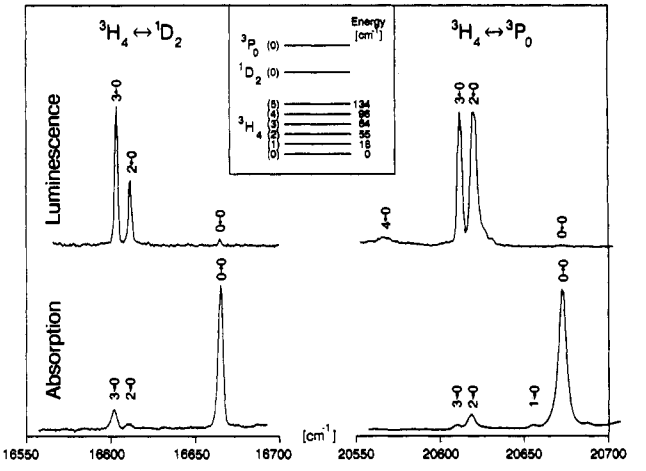

Figure 4. Resonance in unpolarized absorption (30 K) and unpolarized emission (7 K) of the transitions $^3H_4 \leftrightarrow {}^1D_2$ and $^3H_4 \leftrightarrow {}^3P_0$ in $Pr(CH_3COO)_3 \cdot H_2O$. The insert shows the designation and energy of the crystal-field components.

whereas in the diluted one it is only 20%.

Visible luminescence spectra of $Pr(CD_3COO)_3 \cdot D_2O$ at 7 K are presented in Figure 2. The luminescence is dominated by transitions from $^3P_0$. The insert shows a comparison in the yellow region of $Pr(CH_3COO)_3 \cdot H_2O$ with the doped $Ce(CH_3COO)_3 \cdot H_2O$:1% Pr^{3+} system. The ($^1D_2 \rightarrow {}^3H_4/{}^3P_0 \rightarrow {}^3H_6$) emission intensity ratio is enhanced by 2–3 orders of magnitude by dilution.

Figure 3 shows Raman spectra of $Pr(CH_3COO)_3 \cdot H_2O$ and $Pr(CD_3COO)_3 \cdot D_2O$ at 7 K. Spectra were recorded for various excitation wavelengths but no λ dependence was found. The transitions in Figure 3 can be identified by a comparison with the vibronic lines in $Gd(CH_3COO)_3 \cdot 4H_2O$[20] and infrared absorption spectra. The most interesting part is the low-energy region up to 350 cm^{-1}, which is dominated by Pr–O bending and stretching modes and which shows a great deal of similarity with the sideband structure of the electronic transition $^3H_4 \rightarrow {}^3P_0$ in absorption; see insert of Figure 3.

The crystal-field splitting of the $^3H_4$ ground state was investigated by temperature-dependent absorption measurements in comparison with luminescence spectroscopy. Figure 4 shows unpolarized absorption spectra of $Pr(CH_3COO)_3 \cdot H_2O$ at 30 K for $^3H_4 \rightarrow {}^1D_2$ and $^3H_4 \rightarrow {}^3P_0$ in the region of the electronic origins with their corresponding luminescence at 7 K. From the coincidence of the lines in absorption and emission and from their temperature dependence in absorption, the four crystal-field levels,

(17) Dieke, G. H. *Spectra and Energy Levels of Rare Earth Ions in Crystals*; Interscience Publishers: New York, 1968.
(18) Richardson, F. R.; Reid, M. F.; Dallara, J. J.; Smith, R. D. *J. Chem. Phys.* **1985**, *83*, 3813.
(19) Hüfner, S. *Optical Spectra of Transparent Rare Earth Compounds*; Academic Press: New York, 1978.
(20) Blasse, G.; Brixner, L. H. *Recl. Trav. Chim. Pays-Bas* **1990**, *109*, 172.

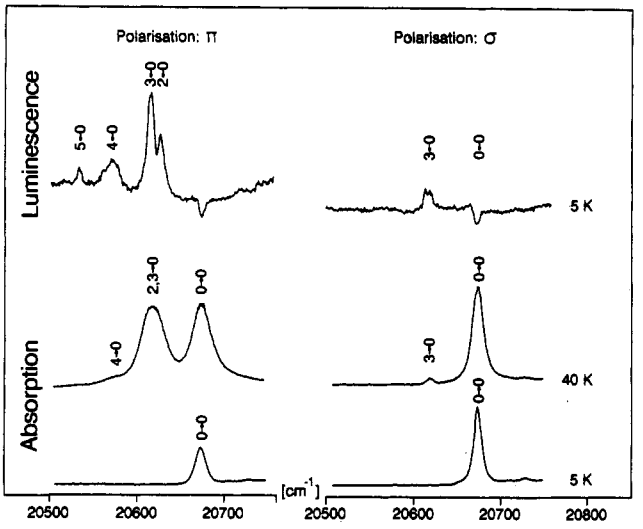

Figure 5. $^3H_4 \leftrightarrow {}^3P_0$ transition in $Pr(CH_3COO)_3 \cdot H_2O$ in π- and σ-polarization at two temperatures.

0, 2, 3, and 4, of the $^3H_4$ ground state can be identified. A fifth level, $^3H_4(1)$ at 18 cm^{-1}, and a sixth level, $^3H_4(5)$ at 134 cm^{-1}, can only be observed in absorption or emission, respectively. Higher energy levels could not be detected due to their intrinsic weakness in emission. The insert in Figure 4 shows the energy splitting pattern of $^3H_4$ derived from the high-resolution spectra.

The $^3P_0 \leftrightarrow {}^3H_4(i)$ transitions are strongly polarized both in absorption and luminescence. Figure 5 shows polarized absorption and luminescence spectra of the electronic origins in $Pr(CH_3COO)_3 \cdot H_2O$ at two temperatures. With the exception of the $0 \leftrightarrow 0$ transition, which is somewhat stronger in σ polarization, all the lines are more intense in π polarization. This is true for both absorption and luminescence, which clearly demonstrates that the luminescence is intrinsic and not due to traps. It is interesting to note that the $^3P_0 \leftrightarrow {}^3H_4(0)$ luminescence line cannot be observed at 5 K. It is fully reabsorbed, and due to some broad background luminescence it is observed as a negative line in Figure 5.

4. Discussion

4.1. Electronic Transitions and $^3H_4$ Crystal-Field Splitting. The properties of trivalent lanthanide ions in solids are dominated by their partially filled inner 4f orbitals. The parity-forbidden electronic transitions within the 4f orbitals give rise to very weak but sharp spectra lines. The electronic states of a lanthanide ion in a solid are well approximated by those of the free ion in Russel–Saunders $^{(2S+1)}L_J$ terms.[21] For the $4f^2$ configuration of Pr^{3+}, we have a $^3H_4$ ground state, and the relevant excited states in the visible part of the spectrum are $^1D_2$, $^3P_0$, $^3P_1$, $^1I_6$, and $^3P_2$ as shown in the insert of Figure 1. With the exception of $^3P_0$ all these states will be split by the crystal field. The order of magnitude of these splittings is 10^2 cm^{-1}. With a site symmetry for Pr^{3+} of C_1 in our acetate, we expect a complete lifting of the $(2J + 1)$ fold degeneracy in each free-ion state. We make no attempt to determine and analyze the crystal-field splittings of all states involved in the spectroscopic transitions. Such analyses have been made for trivalent lanthanide ions in purely octahedral sites in elpasolite halide lattices[18] and for the binary halide lattices.[17] For our 9-fold Pr^{3+} coordination with C_1 site symmetry, a calculation of the crystal-field splittings would be a formidable task, and we restrict our data analysis to an experimental determination of the $^3H_4$ crystal-field splitting (see Figures 4 and 5). The $^3H_4 \leftrightarrow {}^3P_0$ transitions are best suited for this purpose, because $^3P_0$ has no electronic degeneracy and thus remains unsplit in the crystal field. As shown on the left-hand side of Figure 4, the $^3H_4 \leftrightarrow {}^1D_2$ transition can also be used to determine the $^3H_4$ splitting. This is due to the fact that the energy difference between $^1D_2(1)$ and $^1D_2(0)$ is quite big. A total of six out of the possible nine crystal-field levels of $^3H_4$ can be determined; see the insert in Figure 4. Intensities of the various crystal-field transitions vary by orders of magnitude. In our luminescence spectra, we are handicapped by very competitive nonradiative processes, so that the weakest lines remain undetected. In absorption, we need to thermally populate the higher crystal-field levels, and the thermal broadening of the lines above 50 K prevents the detection of weak transitions in that case.

4.2. Nonradiative Relaxation. 4.2.1. Multiphonon Relaxation. The integrated visible luminescence intensity of $Pr(CH_3COO)_3 \cdot H_2O$ can be increased by a factor of 12 by complete deuteration. This is accompanied by an increase of the $^3P_0$ luminescence lifetime from $\tau < 1$ ns for the undeuterated to $\tau \sim 5$ ns for the deuterated acetate. These deuteration effects clearly demonstrate that nonradiative relaxation processes are dominant in the undeuterated compound, and the gain in intensity results from a reduction of the relevant nonradiative relaxation rates. We have to consider the following two nonradiative processes: (i) multiphonon relaxation of an excited Pr^{3+} center and (ii) excitation energy transfer to unintentional killer traps in the lattice. It is hardly conceivable that process ii should be strongly dependent on deuteration. For process i, on the other hand, it is well-established that the highest energy vibrational modes play the dominant part. The principal deuteration effect is due to the replacement of H_2O by D_2O because the O–H bond of the water ligand is closer to Pr^{3+} than the C–H bonds of the acetate ligands. According to the energy-gap law for lanthanide f–f transitions[22]

$$k_{nr} = \beta_{el} e^{-(\Delta E_0 - 2\hbar\omega_{max})\alpha} \quad (1)$$

where k_{nr} is the nonradiative multiphonon relaxation rate at 0 K, ΔE_0 is the energy gap to the next lower electronic state and $\hbar\omega_{max}$ is the energy of the accepting vibrational mode in the first coordination sphere of the Ln^{3+} ion. α and β_{el} are two host-dependent empirical parameters, which range from 3×10^{-3} cm to 4.5×10^{-2} cm and from 3×10^6 s^{-1} to 2×10^8 s^{-1}, respectively.[22] For our calculations we choose mean values for lattices with oxygen coordination; thus $\alpha = 4 \times 10^{-3}$ cm and $\beta_{el} = 10^7$ s^{-1}. This law is usually very well obeyed in lanthanide systems.[22] From eq 1, it is clear that the highest energy vibration is the most likely accepting mode in the multiphonon relaxation process. In our acetate, the O–H stretching vibration is lowered from 3250 to 2470 cm^{-1} upon deuteration; see Figure 3.

The relevant energy gaps for Pr^{3+}, as seen from the diagram in Figure 1, are $^1D_2$–$^1G_4$ (gap 1) and $^3P_0$–$^1D_2$ (gap 2). In our system, they have values of about 7000 and 4000 cm^{-1}, respectively. Compared to the principal energy gaps in other rare-earth ions, these are very small gaps. Considering the presence of 3250-cm^{-1} O–H vibrators in close proximity to the Pr^{3+} ions, it is therefore surprising that luminescence can be observed at all, at least in the undeuterated acetate. Since the $^1D_2$–$^1G_4$ energy gap is almost twice as large as the $^3P_0$–$^1D_2$ gap, we expect a dominance of $^1D_2$ emission in the luminescence spectrum. Figure 2 shows that the actual behavior is opposite: $^3P_0$ emission intensity dominates by at least 2 orders of magnitude. There are two main reasons for this: (i) the nonvalidity of the energy-gap law for such small energy gaps; (ii) the nonradiative cross relaxation of $^1D_2$. The latter mechanism is by far the most important in the undiluted compounds $Pr(CH_3COO)_3 \cdot H_2O$ and $Pr(CD_3COO)_3 \cdot D_2O$, as can be seen in the insert of Figure 2. Pr^{3+} doped into the isostructural host lattice $Ce(CH_3COO)_3 \cdot H_2O$ shows a significantly different luminescence spectrum. In particular, the intensity ratio of $^1D_2$ to $^3P_0$ emission is increased by a factor of 600 compared to that in $Pr(CH_3COO)_3 \cdot H_2O$. There is obviously a highly efficient relaxation mechanism from $^1D_2$ that is not operative in the diluted system. This will be discussed in detail in section 4.2.2.

For a discussion of the multiphonon relaxation processes on a Pr^{3+} single ion, we use the data of the diluted crystal; see the insert in Figure 2. We were not able to measure the lifetime of the $^1D_2 \rightarrow {}^3H_4$ luminescence due to its low intensity. However, from a comparison of the intensity ratios between diluted, undiluted, and

(21) Wybourne, B. G. *Spectroscopic Properties of Rare Earth*; Wiley: New York, 1965.

(22) van Dijk, M. F.; Schuurmans, M. F. H. *J. Chem. Phys.* **1983**, *78*, 5317.

Table I. Lifetimes at 7 K[a]

compound	lifetime τ, s: exptl $^3P_0$	exptl $^1D_2$	calcd from eq 1 $^1D_2$
$Ce(CH_3COO)_3 \cdot H_2O$:1%Pr^{3+}	4×10^{-10}	8×10^{-10}	
$Pr(CH_3COO)_3 \cdot H_2O$	4×10^{-10}	1×10^{-12}	7×10^{-7}
$Pr(CD_3COO)_3 \cdot D_2O$	5×10^{-9}	2×10^{-11}	4×10^{-4}

[a] Experimental column: order of magnitude estimates for the lifetimes of the $^3P_0$ and $^1D_2$ excited states at 7 K using data from the diluted, undiluted, and deuterated compounds and the measured $^3P_0$ lifetime in $Pr(CD_3COO)_3 \cdot D_2O$. Lifetimes in the last column were calculated by using eq 1, with $\alpha = 4 \times 10^{-3}$ cm, $\beta_{el} = 10^7$ s^{-1}, $\hbar\omega_{max,H} = 3250$ cm^{-1}, $\hbar\omega_{max,D} = 2470$ cm^{-1}, $\Delta E_0(^1D_2) = 7000$ cm^{-1}, and $\Delta E_0(^3P_0) = 4000$ cm^{-1}.

deuterated crystals, we can make order of magnitude estimates of the lifetimes τ at 7 K. They are collected in Table I and compared with calculated lifetimes obtained by using eq 1. The calculated values for $^1D_2$ are too high by 5 and 7 orders of magnitude for the undeuterated and deuterated systems, respectively. A calculation of the $^3P_0$ lifetime using eq 1 does not make physical sense since $\Delta E_0 - 2\hbar\omega_{max}$ becomes negative. We conclude that the energy-gap law in (1), which has been very successfully applied in a multitude of trivalent lanthanide systems, does not work in the present case. The reason for this is the small size of the two energy gaps. Choosing ν(O–H) as the effective accepting mode, we have values for $\Delta E_0/\hbar\omega_{max}$ of 2.15 ($^1D_2$), 1.23 ($^3P_0$) and 2.83 ($^1D_2$), 1.62 ($^3P_0$) for the undeuterated and deuterated lattices, respectively. These values are obviously below the limit of validity of the energy-gap law. In the examples quoted in ref 22, the energy-gap law was found to be valid for p values down to 1.4. But for the small energy gaps in our Pr^{3+} systems, the multiphonon relaxation rates depend on whether or not the energy gap can be exactly bridged by first-sphere vibrational modes.

In our case, a nonradiative transition consists of an energy transfer from an electronically excited state of the lanthanide ion to a coupled oscillator, and therefore, donor emission and acceptor absorption have to be in resonance for the transition to take place. Sveshnikova and Ermolaev have derived an expression for the nonradiative relaxation rate k_{nr} based on such a dipole–dipole-induced energy transfer:[23,24]

$$k_{nr} = \sum_i \frac{8.8 \times 10^{-25}\, k_{rad}}{p^4 R_i^6} \int \frac{F(\nu)\,\epsilon(\nu)}{\nu^4}\, d\nu \qquad (2)$$

In eq 2, k_{rad} denotes the total radiative transition rate from the ions excited state to all lower states, p is the number of phonons created by the transition, and R_i is the distance from the lanthanide ion to the center of gravity of the ith oscillator. The crucial factor in eq 2 is the spectral overlap integral, which is calculated from the normalized donor emission spectrum $F(\nu)$ and the vibrational spectrum $\epsilon(\nu)$ of the acceptor. Using eq 2, Sveshnikova and Ermolaev calculated k_{nr} values for lanthanide ions in solutions with an accuracy of 2 orders of magnitude, even for systems with $n = 1.7$ as e.g. for $Nd^{3+}(^4F_{3/2})$ in H_2O.

We do not have enough experimental information to perform such an analysis for our systems. In particular, we do not know all the crystal-field splittings of $^1D_2$ and $^1G_4$, and the relevant infrared emissions $^1D_2 \rightarrow {}^1G_4$ and $^3P_0 \rightarrow {}^1D_2$ could not be measured. But considering the failure of the energy-gap law, we feel that this approach is more reliable in the presence of small energy gaps. However, for a quantitative analysis, it requires a considerable amount of spectroscopic data.

4.2.2. Cross-Relaxation. We concluded from the data in the insert of Figure 2 that there is a nonradiative $^1D_2$ relaxation mechanism in the undiluted compounds with an efficiency 600 times higher than multiphonon relaxation. It has been established for other Pr^{3+} systems[16] that this is a cross-relaxation mechanism as schematically shown below:

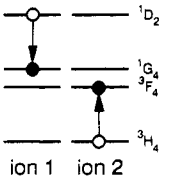

In this process, part of the excitation energy of an initially $^1D_2$ excited ion 1 is transferred to a nearest neighbor ion 2 by a nonradiative mechanism. This is possible because the two energy differences $^1D_2$–$^1G_4$ and $^3F_4$–$^3H_4$ are nearly equal, and the transfer process can proceed by a nearly resonant Dexter mechanism.[25] A possible small energy mismatch can be compensated by one of the numerous low-energy phonon modes. After cross relaxation, both ions will relax to their ground state by multiphonon processes. Neighboring Pr^{3+} ions in the chains of $Pr(CH_3COO)_3 \cdot H_2O$ are separated by 4.4 Å and bridged by acetate groups. These offer favorable pathways for exchange interactions, and the mechanism for the nonradiative excitation transfer by cross relaxation can thus be either an exchange or a multipole–multipole mechanism. It is clear that this relaxation mechanism is suppressed in the diluted system $Ce(CH_3COO)_3 \cdot H_2O$:1% Pr^{3+} since it depends on the existence of a nearest neighbor with a corresponding energy difference. $Ce(CH_3COO)_3 \cdot H_2O$ is an "innocent" host in this respect, since the only f–f excitation has an energy of some 2000 cm^{-1}, far too small to act as an acceptor of the 7000-cm^{-1} $^1D_2 \rightarrow {}^1G_4$ energy. The 4f $\rightarrow$ 5d excited states of Ce^{3+}, on the other hand, have an energy of more than 26 500 cm^{-1} in this lattice, which is higher than that of any of the relevant Pr^{3+} states discussed here.

4.3. Sideband Intensity: Vibronic Transitions and Double Excitations. Most of the bands in the absorption and luminescence spectrum of $Pr(CH_3COO)_3 \cdot H_2O$ have relatively intense sidebands. Since this is not typical for Ln^{3+} spectroscopy, we analyzed it in detail for the low-energy sideband (0–350 cm^{-1}) of the $^3H_4 \rightarrow {}^3P_0$ transition in absorption: 65% and 20% of the total intensity are in the sideband for $Pr(CH_3COO)_3 \cdot H_2O$ and $Ce(CH_3COO)_3 \cdot H_2O$:1% Pr^{3+}, respectively. The upper insert in Figure 1 shows that the sideband structure is not the same in the two crystals. It therefore appears, that in the undiluted compound we have a cooperative effect in addition to a single-ion effect. This is quite similar both phenomenologically and formally to the situation discussed in section 4.2, where an ion-pair process and a single-ion effect contribute to the nonradiative relaxation.

The two effects that contribute to the $^3H_4 \rightarrow {}^3P_0$ sideband intensity are the following: vibronic coupling, a single-ion effect, and exchange or multipole interactions between nearest neighbors, a cooperative effect. Vibronic coupling accounts for about one-third of the total sideband intensity of $Pr(CH_3COO)_3 \cdot H_2O$. In Figure 3, we see a coincidence for some of the sidebands with lines in the Raman spectrum. This is particularly true for the high-energy sidebands at about 220 and 315 cm^{-1}. The insert in Figure 1 shows that these are the principal sidebands that survive after dilution, and we assign them as vibronic sidebands.

Two-thirds of the $^3H_4 \rightarrow {}^3P_0$ sideband intensity of $Pr(CH_3COO)_3 \cdot H_2O$, see insert of Figure 3, particularly the region below 200 cm^{-1}, is due to double electronic excitations. This intensity mechanism is based on the existence of exchange or multipole interactions between nearest neighbors and is therefore only active in the undiluted system.[25] Double excitations involving several electronic states of Pr^{3+} in $PrCl_3$ were observed as early as 1961 by Varsanyi and Dieke.[26] In our case, the occurrence of double excitations in the $^3H_4 \rightarrow {}^3P_0$ sideband structure can be understood as follows. At $T = 0$ K an electronic excitation $^3H_4(0) \rightarrow {}^3P_0$ on one ion is coupled to a $^3H_4(0) \rightarrow {}^3H_4(i)$ ($i = 1$–8) excitation on a neighboring Pr^{3+} ion in the chain. The resulting transition

(23) Sveshnikova, E. B.; Ermolaev, V. L. *Opt. Spektrosc.* **1971**, *30*, 379.
(24) Ermolaev, V. L.; Sveshnikova, E. B. *Chem. Phys. Lett.* **1973**, *23*, 349.
(25) Dexter, D. L. *Phys. Rev.* **1962**, *126*, 1962.
(26) Varsanyi, F.; Dieke, G. H. *Phys. Rev. Lett.* **1961**, *7*, 442.

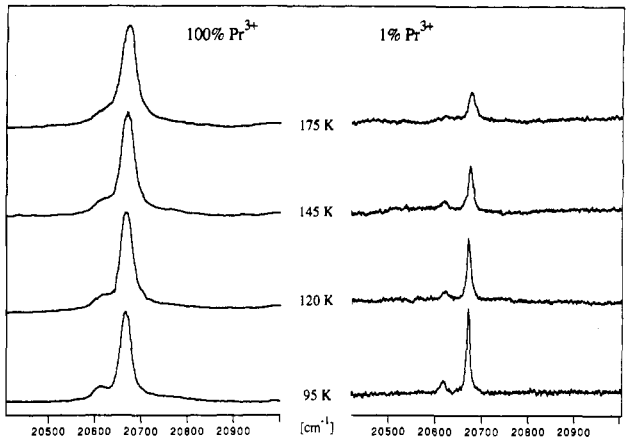

Figure 6. Temperature dependent unpolarized absorption spectra of the $^3H_4 \rightarrow {}^3P_0$ absorption in $Pr(CH_3COO)_3 \cdot H_2O$ and $Ce(CH_3COO)_3 \cdot H_2O$:1% Pr^{3+}.

roughly corresponds to the sum of the two single excitations, thus leading to a high-energy sideband of the $^3H_4(0) \rightarrow {}^3P_0$ electronic origin. In the discussion of the cross-relaxation mechanism, we mentioned earlier that the acetate bridges offer efficient pathways for exchange interaction, and it is therefore likely that such interactions, in addition to multipole interactions, are also active for the double excitations.[27] Figure 6 provides a nice confirmation for the double-excitation mechanism in the undiluted acetate. It shows the $^3H_4 \rightarrow {}^3P_0$ absorptions for both the diluted and undiluted system as a function of temperature. The diluted spectra show the expected decrease with increasing temperature of the $^3H_4(0) \rightarrow {}^3P_0$ line. In contrast, the undiluted crystal shows an increase accompanied by a broadening of this line. This can be understood by contributions, at high temperatures, of the following double excitations: $^3H_4(i) \rightarrow {}^3P_0 + {}^3H_4(0) \rightarrow {}^3H_4(i)$. Independent of i, their energy is roughly equal to the energy of the $^3H_4(0) \rightarrow {}^3P_0$ single-ion origin. The observed broadening is due to the fact that many double excitations with higher as well as lower energy than $^3H_4(0) \rightarrow {}^3P_0$ become possible with increasing temperature.

(27) Gondaira, K. I.; Tanabe, Y. *J. Phys. Soc. Jpn.* **1966**, *21*, 1527.

5. Conclusions

In this investigation, we have shown that long-range energy migration is not observable in $Pr(CH_3COO)_3 \cdot H_2O$ or its deuterated analogue. Localized nonradiative relaxation processes are highly competitive. By chemical variation without variation of the crystallographic structure, deuteration on the one hand and dilution in $Ce(CH_3COO)_3 \cdot H_2O$ on the other, it was possible to identify and analyze the relevant processes in detail. A single-ion multiphonon relaxation mechanism is accompanied by a cooperative cross-relaxation mechanism in the undiluted compounds. Similarly, a single-ion and a cooperative intensity mechanism contribute to the sideband structure of the $^3H_4 \rightarrow {}^3P_0$ absorption in $Pr(CH_3COO)_3 \cdot H_2O$.

Energy migration phenomena in lanthanide acetates with chain structures are not likely to be observable for the Ln^{3+} other than Gd^{3+}, Eu^{3+}, and Tb^{3+}. The latter ions have much larger energy gaps and correspondingly much smaller nonradiative relaxation rates. Energy migration processes may therefore become competitive. The compounds $[Ln(CH_3COO)_2(H_2O)_3]Cl$ (Ln = Gd^{3+}, Eu^{3+}, Tb^{3+}) form chain structures, and we are presently investigating their properties.

Acknowledgment. We thank G. Meyer and T. Schleid for their help with the synthesis and crystal growth and G. Blasse for useful discussions in the data analysis. Financial support by the Swiss National Science Foundation is acknowledged.

Contribution from the Dipartimento di Chimica Inorganica e Metallorganica, Centro CNR, Via Venezian 21, I-20133 Milano, Italy

Electronic and Geometrical Structures of Nitroso Ligands Coordinated to Transition-Metal Atoms. A Nonempirical Theoretical Study of $Pt(PH_3)_2(CF_3NO)$ and $Pt(PH_3)_2(CH_3NO)$

P. Fantucci,* M. Pizzotti, and F. Porta

Received June 5, 1990

The modifications of the molecular geometry and electronic structure of CF_3NO and CH_3NO caused by coordination to a Pt(0) center have been studied by means of nonempirical MO-LCAO theoretical calculations on the model complexes $Pt(PH_3)_2(RNO)$. The η^2 coordination mode of RNO, in which the N-O group acts as a side-on σ-donor and π-acceptor, is found to be more favorable than the η^1 mode, in which only the N atom directly interacts with the metal center. The bonding characteristics of the RNO ligands are compared with those of the isoelectronic dioxygen ligand by investigating the electronic structure of the $Pt(PH_3)_2(\eta^2\text{-}O_2)$ complex.

Introduction

In recent years, the catalytic carbonylation of organo nitro compounds has attracted much interest[1] because of the potential applicability of the catalysts to the industrial processes leading to the preparation of quite a broad class of compounds like amides, amines, carbamates, ureas, and isocyanates. The latter can be obtained in the single-step reaction

$$RNO_2 + 3CO \rightarrow RNCO + 2CO_2$$

which seems particularly interesting because it avoids the use of an energy-demanding, poisonous, and corrosive reagent like phosgene, necessary, on the contrary, in the classical two-step synthesis

$$RNO_2 + 3H_2 \rightarrow RNH_2 + 2H_2O$$

$$RNH_2 + COCl_2 \rightarrow RNCO + 2HCl$$

The formation of isocyanates proceeds in the presence of group VIII metal catalysts at high temperature and pressure. The nitroso compounds RNO can be considered as intermediates of the reaction

$$RNO_2 + CO \rightarrow RNO + CO_2$$

which react further with CO

$$RNO + 2CO \rightarrow RNCO + CO_2$$

The interaction of the nitroso ligands with a group VIII metal center has been studied mainly from an experimental point of view.

(1) Cenini, S.; Pizzotti, M.; Crotti, C. In *Aspects of Homogeneous Catalysis*; Ugo, R., Ed.; D. Reidel: Dordrecht, The Netherlands, 1988; Vol. VI; see also references therein.

0020-1669/91/1330-2277$02.50/0